MIT Open Access Articles

Shortwave and longwave radiative contributions to global warming under increasing CO[subscript 2]

Massachusetts Institute of Technology

Shortwave and longwave radiative contributions to global warming under increasing CO₂

Aaron Donohoe[a,1], Kyle C. Armour[a], Angeline G. Pendergrass[b], and David S. Battisti[c]

[a]Department of Earth, Atmospheric and Planetary Sciences, Massachusetts Institute of Technology, Cambridge, MA 02139; [b]Advanced Study Program, National Center for Atmospheric Research, Boulder, CO 80307; and [c]Department of Atmospheric Sciences, University of Washington, Seattle, WA 98195

In response to increasing concentrations of atmospheric CO₂, high-end general circulation models (GCMs) simulate an accumulation of energy at the top of the atmosphere not through a reduction in outgoing longwave radiation (OLR)—as one might expect from greenhouse gas forcing—but through an enhancement of net absorbed solar radiation (ASR). A simple linear radiative feedback framework is used to explain this counterintuitive behavior. It is found that the timescale over which OLR returns to its initial value after a CO₂ perturbation depends sensitively on the magnitude of shortwave (SW) feedbacks. If SW feedbacks are sufficiently positive, OLR recovers within merely several decades, and any subsequent global energy accumulation is because of enhanced ASR only. In the GCM mean, this OLR recovery timescale is only 20 y because of robust SW water vapor and surface albedo feedbacks. However, a large spread in the net SW feedback across models (because of clouds) produces a range of OLR responses; in those few models with a weak SW feedback, OLR takes centuries to recover, and energy accumulation is dominated by reduced OLR. Observational constraints of radiative feedbacks—from satellite radiation and surface temperature data—suggest an OLR recovery timescale of decades or less, consistent with the majority of GCMs. Altogether, these results suggest that, although greenhouse gas forcing predominantly acts to reduce OLR, the resulting global warming is likely caused by enhanced ASR.

global warming | climate feedbacks | energy accumulation

Global conservation of energy is a powerful constraint for understanding Earth's climate and its changes. Variations in atmospheric composition that result in a net positive energy imbalance at the top of atmosphere (TOA) drive global warming, with the world ocean as the primary reservoir for energy accumulation (1). In turn, increasing global surface temperature enhances emission of longwave (LW) radiation to space (the Planck response). A schematic of the global energy budget response to a step change in greenhouse gas (GHG) concentrations is illustrated in Fig. 1A: outgoing LW radiation (OLR) initially decreases because of enhanced LW absorption by higher GHG levels; as energy accumulates in the climate system, global temperature rises and OLR increases until the TOA energy balance is restored—when OLR once again balances the net absorbed solar radiation (ASR). In this canonical view of global warming, the net energy accumulation (shaded green area in Fig. 1A) is a consequence of decreased OLR driven by GHG forcing. In contrast, consider a hypothetical step change in solar insolation (Fig. 1B): ASR is increased, and energy accumulates until the climate warms sufficiently that OLR balances the ASR perturbation. In this case, the net energy accumulation (shaded red area in Fig. 1) is a consequence of increased ASR and opposed by the increased OLR (hatched green area in Fig. 1).

Is the present global warming caused by reduced OLR (as in Fig. 1A) or enhanced ASR (as in Fig. 1B)? Anthropogenic radiative forcing is dominated by LW active constituents, such as CO₂ and methane, and shortwave (SW) forcing agents, such as sulfate aerosols, are thought to be acting to reduce ASR compared with their preindustrial levels (2). Reduced OLR, thus,

seems the likely cause of the observed global energy accumulation, although the limited length of satellite TOA radiation measurements precludes determination of the relative contributions of ASR and OLR by direct observation. Trenberth and Fasullo (3) considered global energy accumulation within the ensemble of coupled general circulation models (GCMs) participating in phase 3 of the Coupled Model Intercomparison Project (4) (CMIP3). They report that, under the Special Report on Emission Scenarios A1B emissions scenario, wherein increasing radiative forcing is driven principally by increasing GHG concentrations, OLR changes little over the 21st century and global energy accumulation is caused nearly entirely by enhanced ASR—seemingly at odds with the canonical view of global warming by reduced LW emission to space (outlined in Fig. 1A).

Here, we seek insight into this surprising result. In particular, we examine CO₂-only forcing scenarios as simulated by the CMIP5 ensemble of state of the art GCMs (5). Perturbing CO₂ alone permits a clean partitioning of radiative forcing and radiative response into their respective SW and LW components and allows an investigation into the relative contributions of reduced OLR and enhanced ASR to global energy accumulation. The CMIP5 multi-GCM mean response to a compounding 1% per year CO₂ increase (hereafter, 1% CO₂) is shown in Fig. 1D. Although CO₂ radiative forcing increases approximately linearly in time for 140 y (dotted lines in Fig. 1D), OLR changes little from its preindustrial value, and global energy accumulation is accomplished nearly entirely by increased ASR, consistent with the multi-GCM mean results in the work Trenberth and Fasullo (3). Perhaps even more striking is the response to an abrupt quadrupling of CO₂ (hereafter, 4× CO₂), which is shown in Fig. 1C: OLR initially decreases, like in Fig. 1A, but recovers to its unperturbed (preindustrial) value within only two decades;

Significance

The greenhouse effect is well-established. Increased concentrations of greenhouse gases, such as CO₂, reduce the amount of outgoing longwave radiation (OLR) to space; thus, energy accumulates in the climate system, and the planet warms. However, climate models forced with CO₂ reveal that global energy accumulation is, instead, primarily caused by an increase in absorbed solar radiation (ASR). This study resolves this apparent paradox. The solution is in the climate feedbacks that increase ASR with warming—the moistening of the atmosphere and the reduction of snow and sea ice cover. Observations and model simulations suggest that even though global warming is set into motion by greenhouse gases that reduce OLR, it is ultimately sustained by the climate feedbacks that enhance ASR.
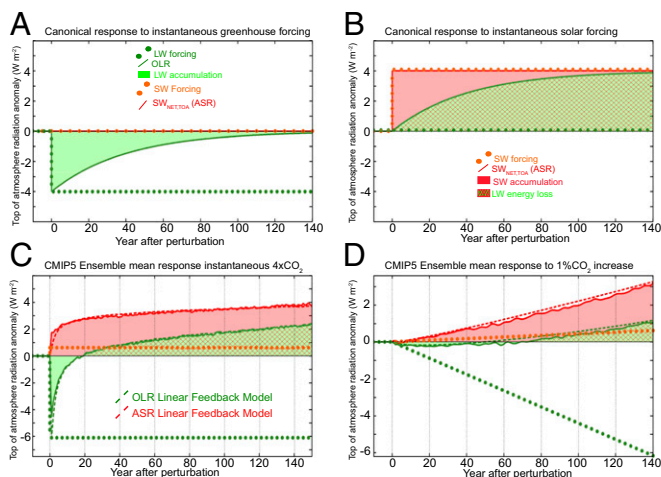

Fig. 1. (*A*) Idealized response of global mean radiation at the TOA to an instantaneous GHG forcing (green dots) assuming no SW feedback and a radiative adjustment e-folding time of 20 y. The green line shows the OLR response (anomaly from preindustrial), and the shaded green area shows the LW energy accumulation. (*B*) The same as in *A* but in response to an instantaneous SW forcing (red dots), with the red line showing the ASR response. In this case, the net energy accumulation is the difference between the SW energy accumulation (the shaded red area) and the LW increase (the hatched green area, where the hatching indicates that the LW response leads to a cooling of the climate system). (*C*) The ensemble average radiative response in the CMIP5 $4\times CO_2$ simulations. The shaded area represents the energy accumulation by SW (red) and LW (green) anomalies, and the hatched area indicates energy loss by enhanced OLR. The dashed red and green lines show the predicted ensemble average ASR and OLR responses from the linear feedback model (Eqs. **1** and **2**). (*D*) The same as in *C* but for the CMIP5 ensemble average radiative response in the 1% CO_2 increase per year simulations (with linear increase in forcing as shown by dotted lines).

beyond this initial adjustment period, energy is lost due to enhanced OLR and gained solely by enhanced ASR.

Here, we propose a simple physical mechanism for this behavior. We show that the simulated global mean OLR and ASR responses (Fig. 1 *C* and *D*) and the short recovery time for OLR in particular can be understood in terms of a linear radiative feedback analysis. Moreover, the diversity of feedbacks across the CMIP5 GCMs explains the range in behavior across the models: in a majority of models, OLR recovers within several decades, and the subsequent global energy accumulation is caused by enhanced ASR; in a minority of models, OLR remains diminished for centuries, and global energy accumulation is driven by reduced OLR. Finally, we show that recent satellite observations constrain radiative feedbacks to be within the regime of relatively fast (approximately decades) OLR recovery under GHG forcing, similar to the majority of CMIP5 GCMs. Altogether, these results suggest that, although GHG forcing acts primarily in the LW, the resulting global warming is fundamentally a consequence of enhanced SW energy accumulation.

SW and LW Contributions to Energy Accumulation

We first consider in more detail the global radiative response of the CMIP5 GCMs to an abrupt GHG forcing ($4\times CO_2$) (shown in Fig. 2). The evolution of OLR anomalies differs remarkably between GCMs (Fig. 2*D*). We characterize this range of responses by the time (τ_{cross}) that it takes for OLR to return to its unperturbed value*; τ_{cross} ranges from 2 to 231 y, with an ensemble mean of 19 y (see Fig. 4*A*).

To interpret these findings, we employ a commonly used linearization of the global TOA energy budget:

$$\frac{d(CT_S)}{dt} = F_{SW} + F_{LW} + (\lambda_{SW} + \lambda_{LW})T_S, \qquad [1]$$

where T_S is the global mean surface temperature anomaly, and C is the time-dependent global heat capacity. Eq. **1** relates the rate of global heat content change to the rate of global TOA energy accumulation, which is given by the sum of SW and LW radiative forcings (F_{SW} and F_{LW}) and radiative responses ($\lambda_{SW}T_S$ and $\lambda_{LW}T_S$) (6). Anomalies in OLR and ASR can further be expressed as

$$ASR = F_{SW} + \lambda_{SW}T_S$$

and

$$-OLR = F_{LW} + \lambda_{LW}T_S. \qquad [2]$$

The radiative feedbacks (λ_{SW} and λ_{LW}) can be estimated for each GCM by linear regression of ASR and OLR (Fig. 2 *C* and *D*) with T_S (Fig. 2*A*) over the period after $4\times CO_2$, wherein radiative forcing is approximately constant (7, 8). Moreover, the LW and SW components of CO_2 forcing (F_{LW} and F_{SW}) can be estimated by the $T_S = 0$ intercept of the regression.[†] Forcing and feedback values for the CMIP5 GCMs ([Table S1](#)) are consistent with those estimated by Andrews et al. (10).

As defined by Eq. **1**, the effective heat capacity C (Fig. 2*B*) is the time-integrated TOA energy accumulation divided by T_S. It has long been recognized that there is no single heat capacity (or characteristic relaxation time) of the climate system (11). Indeed, C increases with time as heat penetrates below the surface mixed layer and into the ocean interior (12–15). For the CMIP5 GCMs, C corresponds to an equivalent ocean depth of 50 m in the first decade after $4\times CO_2$ and increases over time, reaching an equivalent depth of several hundred meters after a century (Fig. 2*B*). The time evolution of C together with values of SW and LW feedbacks and forcing permit an iteration of Eq. **1** that accurately reproduces the surface temperature response T_S of each GCM (Fig. 2*A*). ASR and OLR predicted by Eq. **2** are in excellent agreement with their respective responses following $4\times CO_2$ (Fig. 2 *C* and *D*) and account for the vast majority (99%) of the variance in τ_{cross} across the models. Thus, a simple representation of climate feedbacks (Eqs. **1** and **2**) is all that is needed to understand the response of ASR and OLR under GHG forcing.

Insight into the GCM behavior can be gained by considering the values of ASR and OLR required to reach TOA energy balance (equilibrium) with an imposed GHG forcing. If forcing and feedbacks acted only in the LW (as in Fig. 1*A*), the OLR anomaly would increase from a value of $-F_{LW} = 0$ after $4\times CO_2$ (Eq. **2**), and global energy accumulation would be driven entirely by reduced OLR. In the multi-GCM mean, however, there is a substantial positive SW feedback of $\lambda_{SW} = 0.6$ W m^{-2} K^{-1} in addition to the negative LW feedback of $\lambda_{LW} = -1.7$ W m^{-2} K^{-1} (Fig. 3*A*). As a result, ASR increases with warming, contributing to global energy accumulation. Moreover, the positive λ_{SW} amplifies the equilibrium temperature response by a gain factor[‡] ($G_{\lambda_{SW}}$) of ~1.5 relative to a system with LW feedbacks only, where

$$G_{\lambda_{SW}} \equiv 1/(1 + \lambda_{SW}/\lambda_{LW}). \qquad [3]$$

The multi-GCM mean OLR must, therefore, increase by $1.5F_{LW}$ after $4\times CO_2$ (from $-F_{LW}$ to $0.5F_{LW}$) to reach equilibrium

---

*Note that, if OLR remains below its unperturbed value for the entirety of the 150-y simulation, we estimate τ_{cross} by linear extrapolation over the final century of the simulations. In this case, τ_{cross} should be considered a metric for the GHG forcing ameliorated by the response, because it is possible that OLR may never return to its unperturbed value.

[†]Radiative forcing by this method includes both the direct radiative forcing by the GHG and the effect of any tropospheric adjustments that occur on timescales of days to weeks (9).

[‡]We note that this gain factor differs from the commonly used feedback gain defined as the amplification of the equilibrium temperature response by radiative feedbacks (e.g., water vapor and surface albedo) relative to the response with the Planck feedback only (16, 17).
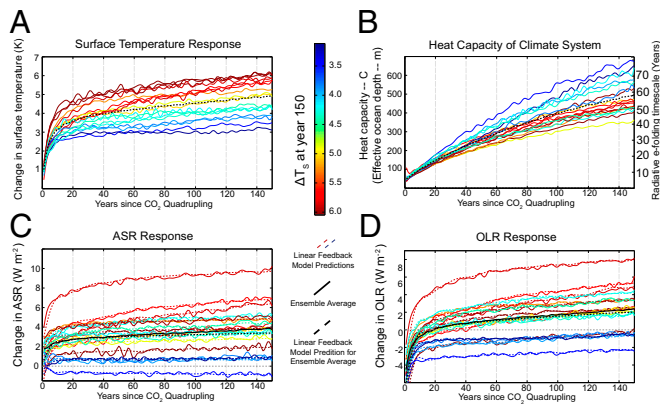
Fig. 2. (A) Time series of global mean surface temperature change in the CMIP5 4× CO_2 simulations. The individual models are indicated by the colored lines and color-coded by the temperature change at year 150 (the color bar is provided in the middle of the figure). The ensemble average is shown by the dashed black line. (B) The heat capacity of the climate system defined as the global time-integrated energy accumulation divided by surface temperature (Eq. 1) given in units of the effective depth of a column of ocean (left axis) and units of radiative e-folding timescale (negative of heat capacity divided by the ensemble mean net radiative feedback $\lambda_{LW} + \lambda_{SW} = -1.1$ W m^{-2} K^{-1}; right axis). (C) Time series of the ASR response, where the solid lines are the GCM values and the dashed lines are the predictions of the linear feedback model (Eqs. 1 and 2) using the GCM-specific heat capacity, forcings, and feedbacks. The solid black line is the ensemble mean of the GCM, and the dashed black line is the prediction of the linear feedback model using the ensemble average heat capacity, forcings, and feedbacks. (D) The same as in C except for the OLR response.

(Eq. 2). Thus, OLR returns to its unperturbed value when $1 F_{LW}/1.5 F_{LW} \approx 66\%$ of the equilibrium temperature response has been realized. We estimate this timescale below. If we assume, for the moment, that the warming over the first several decades can be approximated with a constant heat capacity C, Eq. 1 can be readily solved for the time evolution of the surface temperature, giving

$$T_S = G_{\lambda_{SW}} \frac{F_{LW}}{\lambda_{LW}} \left(e^{\frac{-t}{\tau}} - 1 \right), \qquad [4]$$

where

$$\tau = -\frac{C}{\lambda_{LW} + \lambda_{SW}}. \qquad [5]$$

From Eq. 4, the ~66% of the equilibrium temperature change required for OLR to recover to preindustrial values will be achieved at approximately time τ; that is, τ_{cross} is approximately equal to τ in the ensemble average. If we take the ensemble mean of C over the first century of the 4× CO_2 simulations as an upper bound on its value over the first several decades ($C \approx 250$ m from Fig. 2B), then Eq. 5 provides an upper bound on τ. For ensemble mean feedback values (Table S1), Eq. 5 gives $\tau \approx 29$ y, which is in good agreement with the CMIP5 ensemble mean OLR recovery timescale $\tau_{cross} = 19$ y. For all times after τ_{cross}, energy is lost through enhanced LW emission, and energy accumulation is solely due to enhanced ASR. Thus, the relative contributions of SW and LW anomalies to the total energy accumulation depend directly on the time that it takes for OLR to return to and cross its unperturbed value (τ_{cross}). In the multi-GCM mean, OLR takes only two decades to recover, and thus, energy accumulation is due primarily to enhanced ASR.

What, then, sets the large range of τ_{cross} across the CMIP5 GCMs? While a substantial fraction of equilibrium warming is achieved within the first several decades in all GCMs (15, 18)—due to the fast response of the surface components of the climate

system (12)—the ASR and OLR responses to warming (and τ_{cross}) depend on the SW and LW feedbacks, which vary substantially (Fig. 3A). The dependence of τ_{cross} on the feedback parameters can be seen explicitly by solving the linear feedback model for τ_{cross} (under the assumption that $F_{SW} = 0$). Substituting Eq. 4 into Eq. 2 and identifying $t = \tau_{cross}$ as the time when OLR = 0 gives $F_{LW} = F_{LW} G_{\lambda_{SW}} (e^{\tau_{cross}/\tau} - 1)$, which has the solution

$$\tau_{cross} = -\tau \ln \left(1 - \frac{1}{G_{\lambda_{SW}}} \right). \qquad [6]$$

Eq. 6 reveals that the OLR recovery time is proportional to (i) the radiative e-folding timescale τ, which is on the order of several decades, and (ii) a factor $\ln(1 - 1/G_{\lambda_{SW}}) = \ln(-\lambda_{SW}/\lambda_{LW})$, which is ≈ 1 in the multi-GCM mean but varies by two orders of magnitude across the GCMs. A positive SW feedback amplifies warming, and thus enhances the OLR response and decreases the timescale for OLR recovery. Moreover, τ_{cross} is far more sensitive to changes in λ_{SW} than λ_{LW} over the parameter space realized in the GCMs (curves in Fig. 3A), suggesting that the intermodel differences in τ_{cross} are primarily controlled by variations in SW feedbacks. This result arises from a fundamental asymmetry in the dependence of OLR on λ_{SW} and λ_{LW}: a more positive λ_{SW} acts to amplify warming, which enhances OLR and decreases τ_{cross}; a less negative λ_{LW} similarly acts to amplify warming, which enhances OLR, but it also diminishes the OLR response per degree T_S change (Eq. 2), altogether driving only small changes in τ_{cross}.

Despite its many simplifications, Eq. 6 provides a reasonable estimate of τ_{cross} as simulated by the GCMs, explaining 66% of the variance across models (Fig. 3A). In particular, it broadly captures the short OLR recovery time in the CMIP5 models with large and positive λ_{SW} values and the long OLR recovery time in models with a near-zero λ_{SW}. There are a few notable exceptions, however, where Eq. 6 predicts a substantially smaller τ_{cross} than is realized. τ_{cross} is underestimated in these models because we have not yet accounted for the SW component of CO_2 forcing, which is substantial in a few GCMs because of the rapid cloud adjustments that occur on timescales faster than surface temperature changes. Analogous to the SW feedback case discussed above, SW forcing amplifies the equilibrium temperature response by an SW forcing gain factor, $G_{F_{SW}}$, relative to the system with LW forcing only:

$$G_{F_{SW}} \equiv 1 + \frac{F_{SW}}{F_{LW}}. \qquad [7]$$

A positive SW forcing amplifies warming, enhancing the OLR response and decreasing τ_{cross}, whereas a negative SW forcing reduces warming, diminishing the OLR response and increasing τ_{cross}. Including the effects of SW feedbacks and forcing together gives a simple extension of Eq. 6, wherein the gains are multiplicative (SI Text):

$$\tau_{cross} = -\tau \ln \left(1 - \frac{1}{G_{\lambda_{SW}} G_{F_{SW}}} \right). \qquad [8]$$

In the multi-GCM mean, F_{SW} is relatively small (Table S1), giving $G_{F_{SW}} \approx 1.1$ and modifying τ_{cross} little from that predicted by Eq. 6. However, in some models, F_{SW} is a substantial fraction of the total CO_2 forcing (Fig. 3B), and thus, it has a large impact on τ_{cross}. With F_{SW} taken into account, Eq. 8 provides an excellent estimate of τ_{cross} as simulated by the GCMs, explaining 78% of the variance across models.

If a constant value $\tau \approx 29$ y is used in Eq. 8, the dependence of τ_{cross} on the feedback and forcing gains can be visualized (curves in Fig. 3B). τ_{cross} has very steep gradients in the region where the product of $G_{\lambda_{SW}}$ and $G_{F_{SW}}$ approaches one, leading to a bimodal distribution of τ_{cross}, with OLR returning to unperturbed values either over a couple decades or at timescales longer than a century.

Although $G_{\lambda_{SW}}$ and $G_{F_{SW}}$ contribute equally to τ_{cross}, $G_{\lambda_{SW}}$ varies by a greater amount than $G_{F_{SW}}$ across the GCMs. Thus, it is SW feedback that most strongly controls the range of τ_{cross} and the relative contributions of OLR and ASR to global energy accumulation. However, in models with a sufficiently negative F_{SW} ($G_{F_{SW}} < 0$), τ_{cross} can be on the order of centuries, even with a large and positive λ_{SW} ($G_{\lambda_{SW}} > 0$). In general, OLR recovers on timescales of centuries in models with either weak SW feedbacks or weak (or negative) SW forcing, and OLR recovers on timescales of several decades in models with moderate SW feedbacks and SW forcing. This result can be further seen by varying only λ_{SW} and F_{SW} in the linear feedback model (Eq. **1**) and setting λ_{LW}, F_{LW}, and C equal to their ensemble mean values. The predicted values of τ_{cross} are in excellent agreement ($R^2 = 0.98$) with those simulated by the GCMs (Fig. 4*A*), except for two models with C much larger than the ensemble mean value. Importantly, allowing only λ_{SW} and F_{SW} to vary between models is sufficient to capture the clear separation between (*i*) those models with τ_{cross} on the order of centuries (black circles in Fig. 4*A*), where global energy accumulation is dominated by reduced OLR, and (*ii*) those models with τ_{cross} on the order of decades (colored

circles in Fig. 4*A*), where global energy accumulation is dominated by enhanced ASR and opposed by enhanced OLR.

With these insights in mind, we return to the relative roles of ASR and OLR in driving global energy accumulation under the 1% CO_2 increase per year scenario, where GHG concentrations increase slowly over time, as in nature, rather than abruptly quadrupling. To quantify the relative roles of enhanced ASR and reduced OLR in transient energy accumulation, we define the SW energy accumulation ratio (SWEAR) to be the ratio of time-integrated energy accumulation via enhanced ASR to the time-integrated net radiative imbalance ($ASR - OLR$) over the 140 y of the 1% CO_2 simulations:

$$\text{SWEAR} = \frac{\int ASR\, dt}{\int (ASR - OLR)\, dt}. \qquad [9]$$

Values of SWEAR vary considerably across the GCMs (Fig. 4*B*), from near zero (energy accumulated primarily by reduced OLR) to near three (energy accumulated by enhanced ASR and lost by enhanced OLR). SWEAR between 0 and 1 indicates energy accumulation through both enhanced OLR and reduced OLR, whereas SWEAR above 0.5 indicates that ASR contributes more than one-half of global energy accumulation. In the multi-GCM mean, SWEAR is 1.1, indicating that OLR changes little and that net energy accumulation is accomplished entirely by enhanced ASR (Fig. 1*D*).

This range of GCM behavior under slowly increasing GHG forcing follows directly from the range of OLR recovery timescales τ_{cross} identified above under an abrupt change in GHGs, which, in turn, is set by intermodel differences in SW feedbacks and forcing. Indeed, the linear feedback model (Eqs. **1** and **2** with parameters estimated from $4\times CO_2$ as described above) iterated forward under 1% CO_2 captures the multi-GCM ASR and OLR response (dashed lines in Fig. 1*D*) and their variations across models. The linear feedback model, thus, also captures the inter-GCM variance in SWEAR (95%), where the vast majority (85%) of the inter-GCM variance can be explained by varying λ_{SW} and F_{SW} only (with λ_{LW}, F_{LW}, and C set to their ensemble means as above) (Fig. 4*B*).

Fig. 4*B* shows a clear separation between models with SWEAR ≤ 0.5 (OLR-dominated) and models with SWEAR ≥ 1 (ASR-dominated). Furthermore, models with SWEAR ≤ 0.5 are those with τ_{cross} on the order of centuries (Fig. 4*B*, black circles), and models with SWEAR ≥ 1 are the same as those with τ_{cross} on the order of decades (Fig. 4*B*, colored circles). This strong dependence of SWEAR on τ_{cross} can be understood by considering the response to 1% CO_2 as the superposition of many responses to an instantaneous CO_2 forcing, each initiated at a different time. More formally, the time (τ_{ramp}) at which OLR returns to its unperturbed value in response to a linear increase in CO_2 forcing can be approximated by (*SI Text*)

$$\tau_{ramp} = \frac{\tau}{1 - \dfrac{1}{G_{\lambda_{SW}}\, G_{F_{SW}}}} = \tau e^{\tau_{cross}/\tau}. \qquad [10]$$

For models with τ_{cross} on the order of decades, τ_{RAMP} is also on the order of decades, and SWEAR is large. For models with τ_{cross} on the order of a century, τ_{RAMP} is on the order of several centuries, and SWEAR is small. Altogether, τ_{cross} explains 83% of the inter-GCM variance in SWEAR.

Observational Constraints on SW and LW Energy Accumulation

Global mean surface temperature has increased by about 0.85 K since the pre-industrial period (19) due to a global TOA energy accumulation driven by anthropogenic GHG emissions. Estimates
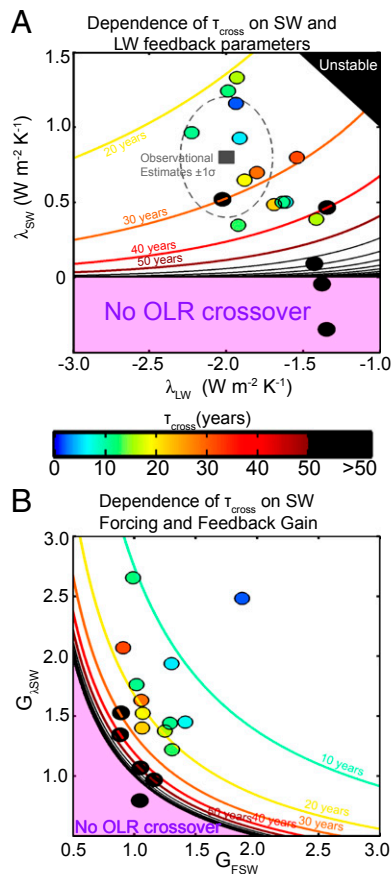

Fig. 3. (*A*) Contours show the sensitivity of τ_{cross} to LW and SW feedback parameters (λ_{LW} and λ_{SW}) in the linear feedback model (Eq. **6**) assuming the forcing is all in the LW and using a time-invariant heat capacity of 250-m ocean depth equivalent—the GCM mean over the first century. The shaded black region is the parameter space over which no equilibrium solution exists, and the shaded pink region is the parameter space over which the OLR never returns to its unperturbed value. The individual GCM results are given by the circles, which are color-coded by τ_{cross} (the color bar is provided in the middle of the figure). The gray ellipse and the dashed lines represent the observational estimates of λ_{LW} and $\lambda_{SW} \pm 1$ SD (σ). (*B*) The sensitivity of τ_{cross} to the SW forcing gain ($G_{F_{SW}}$) and SW feedback gain ($G_{\lambda_{SW}}$) assuming $\tau \sim 29$ y (the GCM mean over the first century) in Eq. **8**.
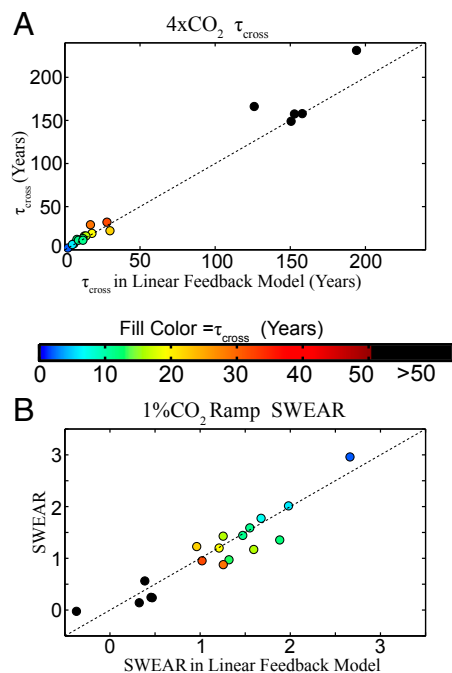
Fig. 4. (*A*) Scatterplot of τ_{cross} in the CMIP5 $4\times CO_2$ simulations and those predicted by the linear feedback model (Eq. **8**) using the GCM-specific λ_{SW} and F_{SW} the GCM ensemble average λ_{LW}, F_{SW}, and heat capacity. The fill color of each circle indicates the τ_{cross} of each GCM in the $4\times CO_2$ simulation. The black dashed line is the 1:1 line. (*B*) The same as in *A* except for that scatterplot is of the SWEAR value in the 1% CO_2 increase per year simulations.

of the rate of global heat content change based on ocean temperature measurements indicate that the current TOA energy accumulation is on the order of 0.5–1 W m^{-2} (20, 21). Is the observed energy accumulation caused by reduced OLR or enhanced ASR? The limited accuracy and length of continuous satellite measurements of Earth's radiative budget (22–24) preclude direct determination of anomalies in OLR and ASR. However, the covariance of SW and LW radiation fluxes with global mean surface temperature over the satellite era permits an estimate of λ_{SW} and λ_{LW} (25). Moreover, given the arguments developed above, these feedback parameters can be used to estimate the relative contributions of ASR and OLR anomalies to the present day global energy accumulation.

Murphy et al. (25) estimated λ_{SW} and λ_{LW} using 6 y of data (2000–2005) from the Clouds and the Earth's Radiant Energy System Energy Balance Filled Project (24). Here, we extend these calculations with the now 14 y (2000–2013) of continuous satellite data and further account for changes in the global radiative forcing of stratospheric aerosols (26) and GHGs (27) over this period[§] (details in *SI Text*); λ_{SW} and λ_{LW} are calculated from the linear regression of monthly anomalies in forcing-adjusted ASR and OLR on monthly surface temperature anomalies (Fig. S2) from three different datasets: (*i*) the National Centers for Environment Prediction reanalysis surface air temperature (31), (*ii*) the Goddard Institute for Space Studies Surface Temperature Analysis (32), and (*iii*) the adaptation by Cowtan and Way (33) of the Climactic Research Unit of the United Kingdom Met Office's Hadley Center (34) surface temperature (version 4). The average of all calculations gives $\lambda_{SW} = 0.8 \pm 0.4$ and $\lambda_{LW} = -2.0 \pm 0.3$ W m^{-2} K^{-1}, where uncertainties represent 1 SD (additional details in *SI Text*). These feedback values are in good agreement with those simulated by the

CMIP5 models, although λ_{SW} is at the upper end of the GCM range (Fig. 3*A*).

We can further estimate the effective global heat capacity *C* from observations by regressing global heat content anomalies [from ocean temperature measurements (35)] onto global mean surface temperature anomalies over the period 1970–2013 (Fig. S3), of which reliable ocean observations exist (20). This calculation gives an average value of $C = 90 \pm 30$ m of equivalent ocean depth, consistent with previous estimates (ref. 36 and references therein) and values over the first few decades of the CMIP5 simulations (Fig. 2*B*). Together, these observational estimates of the feedbacks and heat capacity can be used to estimate the Earth's natural timescale for radiative damping (τ) and OLR recovery (τ_{cross}) after a CO_2 increase: from Eqs. **5** and **6**, $\tau \approx 9$ y and $\tau_{cross} \approx 10$ y, respectively, consistent with but at the low end of the CMIP5 models because of an SW feedback that is at the high end of the model range. Despite the uncertainties in λ_{SW} and λ_{LW}, observations constrain the OLR recovery timescale to be on the order of decades (Fig. 3*A*), and thus, global warming in response to CO_2 forcing is expected to be a consequence of enhanced ASR.

We note that the above analysis assumes that CO_2 forcing acts predominantly in the LW. Although there are currently no direct observations of the SW component of CO_2 forcing induced by rapid cloud adjustments, Eq. **8** suggests that this SW forcing component would have to cancel a substantial fraction (>40%) of the LW component of CO_2 forcing before τ_{cross} becomes greater than several decades. If we use the CMIP5 GCMs as a guide to the range of possibilities, the SW component of CO_2 forcing cancels at most about 20% of the LW component and is more likely to substantially add to the total forcing (Fig. 3*B*), which would further reduce the timescale for OLR recovery and contribute to energy accumulation by enhanced ASR.

The short timescale τ_{cross} suggests that, if anthropogenic radiative forcing had acted predominantly in the LW and increased somewhat linearly over the last century, OLR would have recovered within a decade or so (Eq. **10**), beyond which time global energy accumulation would continue because of enhanced ASR. However, given a present GHG forcing of about 2.8 W m^{-2} (37), the increase in global surface temperature of about 0.85 K above preindustrial temperatures, and the observational estimate of λ_{LW}, Eq. **2** suggests an anomalous OLR of ≈ -0.8 W m^{-2}, implying that OLR is still contributing to global energy accumulation. This apparent discrepancy can be attributed to the effects of tropospheric aerosols, which are acting to reduce global warming (and thus, OLR) through a negative SW radiative forcing on the order of 1 W m^{-2} (although with large uncertainty) (37). Eq. **2** and our observational estimate of λ_{SW} then suggest an anomalous ASR of ≈ -0.2 W m^{-2} in the current climate. Altogether, these estimates imply that the current global energy accumulation is still dominated by decreased OLR. However, they also suggest that a transition to a regime of global energy accumulation dominated by enhanced ASR could occur with only 0.5 K global warming above present—by the middle of the 21st century if warming trends continue as projected.

Discussion and Conclusions

We have shown that, in most climate models, the OLR reduction associated with GHG forcing is alleviated within only a few decades and that the subsequent energy accumulation (and thus, global warming) is caused entirely by enhanced ASR. However, in some models, the OLR response is much slower. The range of model behaviors is readily understood in terms of a simple, linear feedback framework: positive SW feedbacks demand that ASR increases with warming and that OLR must ultimately become greater than its unperturbed value to achieve global energy balance with an imposed radiative forcing. The OLR recovery timescale is typically on the order of decades due to the fast response timescale of the surface components of the climate system and the negative LW feedbacks that strongly increase OLR with warming. Observational constraints also suggest an OLR recovery timescale on the order of decades. However, the current

---

[§]We do not account for changes in the radiative forcing of tropospheric aerosols since they have not changed substantially over this time (28–30).

Donohoe et al.

global energy imbalance seems to be dominated by reduced OLR because of the substantial SW forcing associated with anthropogenic tropospheric aerosols, which have directly reduced ASR and indirectly reduced OLR by curtailing global warming.

The feedback analysis used here ignores time dependence (38) and other nonlinearities in climate feedbacks (39). Although both may be important for the details of the response, our results show that the OLR recovery timescale and the relative contributions of ASR and OLR to energy accumulation are largely governed by linear feedbacks (Fig. 4). At times, we simplified the analysis by assuming a constant effective global heat capacity (C) and associated single timescale of temperature response to forcing (τ). Although C increases over time (Fig. 2B) and there are, of course, multiple timescales of climate response (12, 15), accounting for these details (e.g., by representing a deep ocean heat capacity) makes no substantive changes to our results and conclusions. Indeed, surface temperature increases quickly after a CO_2 perturbation—much of the equilibrium temperature response is realized within the first few decades in all of the GCMs (Fig. 2A)—and the timescale of OLR recovery is most sensitive to the relative magnitudes of λ_{SW} and λ_{LW}. Moreover, when using a constant C, we have chosen a value that leads to a slight overestimate (underestimate) of τ_{cross} when τ_{cross} is small (large), providing an overall conservative estimate of τ_{cross} (Fig. 4A).

Although the differences in λ_{SW} across the CMIP5 models are primarily caused by differences in SW cloud feedbacks (40), the ensemble average value $\lambda_{SW} = 0.6$ W m^{-2} can be attributed to two robust and well-understood consequences of a warmer world: (i) the enhanced SW absorptivity of a moistened atmosphere (41) and (ii) the enhanced SW reflection associated with less-extensive snow and sea ice cover. SW absorption in the atmosphere leads to enhanced ASR by reducing the downwelling radiation incident on the top of clouds and the surface (42). Using radiative kernels (43, 44) and the changes in specific humidity in the CMIP5 4× CO_2 forcing experiments, we calculate an SW water vapor feedback of $+0.3 \pm 0.1$ W m^{-2} K^{-1}. The SW surface albedo feedback has a value of $+0.3 \pm 0.1$ W m^{-2} K^{-1} (43, 45). Thus, the positive λ_{SW} of the CMIP5 ensemble average and the resulting energy accumulation by enhanced ASR under GHG forcing can be expected based only on the robust physics of the water vapor feedback and the surface albedo feedback in the absence of any changes in clouds. Only if the SW cloud feedback is large and negative could the λ_{SW} become small and the resulting energy accumulation be dominated by reduced OLR. Instead, observations constrain λ_{SW} to be at the upper end of the CMIP5 range, implying that OLR recovers quickly in response to GHG forcing and that global warming is driven by enhanced ASR.

1. Levitus S, et al. (2001) Anthropogenic warming of Earth's climate system. *Science* 292(5515):267–270.
2. Collins W, et al. (2006) Radiative forcing by well-mixed greenhouse gases: Estimates from climate models in the intergovernmental panel on climate change (ipcc) fourth assessment report (ar4). *J Geophys Res* 111(D14):D14317.
3. Trenberth KE, Fasullo JT (2009) Global warming due to increasing absorbed solar radiation. *Geophys Res Lett* 36(7).
4. Meehl GA, et al. (2007) The WCRP CMIP3 multi-model dataset: A new era in climate change research. *Bull Am Meteorol Soc* 88(9):1383–1394.
5. Taylor K, Stouffer R, Meehl G (2012) An overview of cmip5 and the experiment design. *Bull Am Meteorol Soc* 93(4):485–498.
6. Budyko M (1969) The effect of solar radiation variations on the climate of the earth. *Tellus B Chem Phys Meteorol* 21(5):611–619.
7. Gregory JM, et al. (2004) A new method for diagnosing radiative forcing and climate sensitivity. *Geophys Res Lett* 31(3):L032051.
8. Gregory J, Webb M (2008) Tropospheric adjustment induces a cloud component in co₂ forcing. *J Clim* 21(1):58–71.
9. Cao L, Bala G, Caldeira K (2012) Climate response to changes in atmospheric carbon dioxide and solar irradiance on the timescale of days to weeks. *Environ Res Lett* 7(3):03415.
10. Andrews T, Gregory J, Webb M, Taylor K (2012) Forcing, feedbacks and climate sensitivity in cmip5 coupled atmosphere-ocean climate models. *Geophys Res Lett* 39(9):L09712.
11. Crowley TJ, North GR (1988) Abrupt climate change and extinction events in Earth history. *Science* 240(4855):996–1002.
12. Held I, et al. (2010) Probing the fast and slow components of global warming by returning abruptly to preindustrial forcing. *J Clim* 23(9):2418–2427.
13. Kim K, North G, Huang J (1992) On the transient response of a simple coupled climate system. *J Geophys Res* 97(D9):10069–10081.
14. Wigley T, Raper S (1987) The thermal expansion of sea water associated with global warming. *Nature* 330(6144):127–131.
15. Kostov Y, Armour KC, Marshall J (2014) Impact of the atlantic meridional overturning circulation on ocean heat storage and transient climate change. *Geophys Res Lett* 41(6):2108–2116.
16. Roe G (2009) Feedbacks, time scales, and seeing red. *Annu Rev Earth Planet Sci* 37:93–115.
17. Hansen J, Lacis A, Rind D, Russell G, Stone P (1984) Climate sensitivity: Analysis of feedback mechanisms. *Climate Processes and Climate Sensitivity*, eds Hansen JE, Takahashi T (American Geophysical Union, Washington).
18. Caldeira K, Myhrvold N (2013) Projections of the pace of warming following an abrupt increase in atmospheric carbon dioxide concentration. *Environ Res Lett* 8(3):34039–34040.
19. Hartmann D, et al. (2013) *Climate Change 2013: The Physical Science Basis. Contribution of Working Group I to the Fifth Assessment Report of the Intergovernmental Panel on Climate Change*, eds Stocker T, et al. (Cambridge Univ Press, Cambridge, UK), Chap 2.
20. Trenberth KE, Fasullo JT, Kiehl J (2009) Earth's global energy budget. *Bull Am Meteorol Soc* 90(3):311–324.
21. Loeb NG, et al. (2012) Observed changes in top-of-the-atmosphere radiation and upper-ocean heating consistent within uncertainty. *Nat Geosci* 5(2):110–113.
22. Barkstrom, et al. (1989) Earth radiation budget (erbe) archival and april 1985 results. *Bull Am Meteorol Soc* 70(10):1254–1262.
23. Wielicki B, et al. (1996) Clouds and the earth's radiant energy system (CERES): An earth observing system experiment. *Bull Am Meteorol Soc* 77(5):853–868.
24. Loeb NG, et al. (2009) Towards optimal closure of the earth's top-of-atmosphere radiation budget. *J Clim* 22(3):748–766.
25. Murphy DM, et al. (2009) An observationally based energy balance for the earth since 1950. *J Geophys Res* 114(D17):16.
26. Solomon S, et al. (2011) The persistently variable "background" stratospheric aerosol layer and global climate change. *Science* 333(6044):866–870.
27. Masarie MPT (1995) Extension and integration of atmospheric carbon dioxide data into a globally consistent measurement record. *J Geophys Res* 100(D6):11593–11610.
28. Murphy DM (2013) Little net clear-sky radiative forcing from recent regional redistribution of aerosols. *Nat Geosci* 6(4):258–262.
29. Carslaw KS, et al. (2013) Large contribution of natural aerosols to uncertainty in indirect forcing. *Nature* 503(7474):67–71.
30. Stevens B (2013) Aerosols: Uncertain then, irrelevant now. *Nature* 503(7474):47–48.
31. Kalnay E, et al. (1996) The NCEP/NCAR 40-year reanalysis project. *Bull Amer Meteor Soc* 77(3):437–471.
32. Hansen J, Ruedy R, Glascoe J, Sato M (1999) Giss analysis of surface temperature change. *J Geophys Res* 104(D24):30997–31022.
33. Cowtan K, Way R (2014) Coverage bias in the hadcrut4 temperature series and its impact on recent temperature trends. *Quart J R Meteor Soc* 140(683):1935–1944.
34. Morice CP, Kennedy J, Rayner N, Jones P (2012) Quantifying uncertainties in global and regional temperature change using an ensemble of observational estimates: The hadcrut4 dataset. *J Geophys Res* 117(D8):D08101.
35. Antonov J, et al. (1998) *World Ocean Atlas 1998 Vol. 1: Temperature of the Atlantic Ocean* (National Oceanographic Data Center, Boulder, CO).
36. Schwartz S (2007) Heat capacity, time constant, and sensitivity of earth's climate system. *J Geophys Res* 112(D24):D15103.
37. Myhre G, et al. (2013) Anthropogenic and Natural Radiative Forcing. *Climate Change 2013: The Physical Science Basis. Contribution of Working Group I to the Fifth Assessment Report of the Intergovernmental Panel on Climate Change*, eds Stocker T, et al. (Cambridge Univ Press, Cambridge, United Kingdom).
38. Armour K, Bitz C, Roe G (2013) Time-varying climate sensitivity from regional feedbacks. *J Clim* 26(13):4518–4534.
39. Feldl N, Roe G (2013) The nonlinear and nonlocal nature of climate feedbacks. *J Clim* 26:8289–8304.
40. Bony S, et al. (2006) How well do we understand climate change feedback processes? *J Clim* 19(21):3445–3482.
41. Donohoe A, Battisti D (2013) The seasonal cycle of atmospheric heating and temperature. *J Clim* 26(14):4962–4980.
42. Donohoe A, Battisti D (2011) Atmospheric and surface contributions to planetary albedo. *J Clim* 24(16):4401–4417.
43. Soden B, Held I (2006) An assessment of climate feedbacks in coupled ocean-atmosphere models. *J Clim* 19(14):3354–3360.
44. Previdi M (2010) Radiative feedbacks on global precipitation. *Environ Res Lett* 5(2):025211.
45. Collins R (2013) Surface albedo feedbacks from climate variability and change. *J Geophys Res* 118(7):2827–2834.

EARTH, ATMOSPHERIC, AND PLANETARY SCIENCES